Environ Sci Pollut Res (2016) 23:1471–1481
DOI 10.1007/s11356-015-5143-x

RESEARCH ARTICLE

# Oxidation of elemental mercury by modified spent $TiO_2$-based SCR-De$NO_x$ catalysts in simulated coal-fired flue gas

**Lingkui Zhao**[1,2] · **Caiting Li**[1,2] · **Xunan Zhang**[1,2] · **Guangming Zeng**[1,2] · **Jie Zhang**[1,2] · **Yin'e Xie**[1,2]

Received: 10 February 2015 / Accepted: 3 August 2015 / Published online: 15 September 2015


**Abstract** In order to reduce the costs, the recycle of spent $TiO_2$-based SCR-De$NO_x$ catalysts were employed as a potential catalytic support material for elemental mercury ($Hg^0$) oxidation in simulated coal-fired flue gas. The catalytic mechanism for simultaneous removal of $Hg^0$ and NO was also investigated. The catalysts were characterized by Brunauer-Emmett-Teller (BET), scanning electron microscope (SEM), X-ray diffraction (XRD), and X-ray photoelectron spectroscopy (XPS) method. Results indicated that spent $TiO_2$-based SCR-De$NO_x$ catalyst supported Ce-Mn mixed oxides catalyst ($CeMn/SCR_1$) was highly active for $Hg^0$ oxidation at low temperatures. The $Ce_{1.00}Mn/SCR_1$ performed the best catalytic activities, and approximately 92.80 % mercury oxidation efficiency was obtained at 150 °C. The inhibition effect of $NH_3$ on $Hg^0$ oxidation was confirmed in that $NH_3$ consumed the surface oxygen. Moreover, $H_2O$ inhibited $Hg^0$ oxidation while $SO_2$ had a promotional effect with the aid of $O_2$. The XPS results illustrated that the surface oxygen was responsible for $Hg^0$ oxidation and NO conversion. Besides, the $Hg^0$ oxidation and NO conversion were thought to be aided by synergistic effect between the manganese and cerium oxides.

**Keywords** Catalytic oxidation · Manganese oxide · Cerium oxide · Elemental mercury · Low temperature

Responsible editor: Angeles Blanco

**Highlights**
- The spent commercial SCR catalyst was used as a support for $Hg^0$ oxidation.
- $CeMn/SCR_1$ catalyst was highly active for $Hg^0$ oxidation at low temperatures.
- The surface oxygen was responsible for $Hg^0$ oxidation and NO conversion.
- Catalytic activity of $Hg^0$ oxidation and NO conversion was measured.
- The catalytic mechanism of catalysts was also investigated.

✉ Caiting Li
ctli@hnu.edu.cn; ctli3@yahoo.com

[1] College of Environmental Science and Engineering, Hunan University, Changsha 410082, People's Republic of China

[2] Key Laboratory of Environmental Biology and Pollution Control (Hunan University), Ministry of Education, Changsha 410082, People's Republic of China

## Introduction

Coal-fired utility boilers are major anthropogenic sources of mercury emissions (Pirrone et al. 2010). Many countries and environmental researchers have paid considerable attention to mercury (Hg) because of its high volatility, long persistence, and strong biological accumulative properties (Brown et al. 1999). In 2011, the USA announced the Mercury and Air Toxics Standard (MATS) (He et al. 2014). In January 2013, 140 nations adopted the first legally binding international treaty to set enforceable limits on emissions of mercury and exclude, phase out, or restrict some products that contain mercury (Auzmendi-Murua et al. 2014).

Many technologies have been used for mercury control in coal combustion flue gas, including activated carbon injection (ACI), catalytic oxidation, photochemical oxidation, and existing air pollution control devices (APCDs) (Srivastava et al. 2006). Catalytic oxidation of elemental mercury ($Hg^0$) could greatly enhance mercury capture efficiency using currently available pollution control devices such as wet scrubbers (Ji et al. 2008). Compared to activated carbon injection, combining $Hg^0$ oxidation with wet flue gas desulfurization (WFGD) is considered as a promising method for mercury removal due to its lower cost. With extensive application in coal-fired power plants, selective catalytic reduction (SCR) technology could control $NO_x$ emission as well as exhibit the co-benefit of promoting $Hg^0$ oxidation. Many studies have

evaluated the performance of the SCR catalysts on $Hg^0$ oxidation (Cao et al. 2008; Kamata et al. 2008; Pudasainee et al. 2010; Yan et al. 2011). However, the commercial $V_2O_5$-$WO_3(MoO_3)/TiO_2$ catalyst has the disadvantages of high reaction temperature (573–673 K) (Zhibo et al. 2013). Moreover, the high concentration of dust in the flue gas reduces its performance and longevity at this temperature (Zhang et al. 2012). Accordingly, in order to avoid the cost for reheating the flue gas and the deactivation by high concentration of dust, it is desirable to develop a novel SCR catalyst with high catalytic activity at low temperatures. $MnO_x$-based catalysts (He et al. 2013; Li et al. 2012; Qu et al. 2014; Wang et al. 2014; Wiatros-Motyka et al. 2013) have been proposed as economical low temperature SCR catalysts for $NO_x$ removal and $Hg^0$ oxidation. It has been widely studied owing to their excellent capture activity, easy manufacturing, and low cost. Ji et al. (Ji et al. 2008) synthesized a novel $MnOx/TiO_2$ catalyst and found NO conversion and $Hg^0$ capture could achieve 97 and 90 %, respectively. Moreover, Li et al. (2010) reported that the $Hg^0$ oxidation efficiency over MnOx/alumina and modified MnOx/alumina catalysts was more than 90 %. Currently, $CeO_2$ has been widely studied as an oxygen provider for heterogeneous catalytic reactions due to its oxygen storage capability by storing or releasing O via the $Ce^{4+}/Ce^{3+}$ redox couple (Shen et al. 2014a; Shen et al. 2014b; Zhang et al. 2013). Significantly, cerium oxides provide oxygen to manganese oxides at low temperatures, which promoted the oxidation activity of manganese (He et al. 2014; Larachi et al. 2002). In particular, Ce-Mn mixed oxide was found to be an excellent low-temperature SCR catalyst (Li et al. 2012; Wu et al. 2008). Li et al. (2012) reported that $TiO_2$ supported Mn-Ce mixed oxides (Mn-Ce/Ti) was highly active for $Hg^0$ oxidation at low temperatures (150–250 °C) under both simulated flue gas and SCR flue gas. He et al. (2014) investigated Ti-pillared-clay supported MnOx-$CeO_2$ mixed oxide as catalysts for $Hg^0$ capture. The results found that the catalyst exhibited high $Hg^0$ adsorbent and catalytic oxidant in the absence of HCl. Besides, the addition of $CeO_2$ could significantly enhance the sulfur resistance and water resistance (Wang et al. 2014). Consequently, Mn-Ce mixed oxide has been recently developed as a SCR catalyst with extraordinarily high activity for $NO_x$ removal and $Hg^0$ oxidation.

It is worth noting that the $TiO_2$-based SCR-$DeNO_x$ catalysts ($V_2O_5$-$WO_3/TiO_2$) usually suffer some types of deactivation during the practical application, such as poisoning, fouling, thermal degradation, and vapor compound formation (Shang et al. 2012). As a result, $TiO_2$-based SCR catalysts are usually in operation for 3 years until the catalytic performance is finally deteriorated. Subsequently, the spent $TiO_2$-based SCR catalyst is either disposed in landfill or recycle. The recycle of catalyst is considered as the best approach due to its cost-saving and environment-friendly benefit. Some works have been done to overcome the drawback of SCR-DeNOx catalysts, including washing by water and acid solution, thermal regeneration, and reductive regeneration (Guo et al. 2008; Khodayari and Odenbrand 2001; Shang et al. 2012). Therefore, the novel development of spent $TiO_2$-based SCR-$DeNO_x$ catalyst as a potential catalytic support material could present a more environmentally and financially sound option for simultaneous removal of $Hg^0$ and NO in conventional coal-fired power plants.

This work attempts to reuse the spent $TiO_2$-based SCR catalyst. The spent $TiO_2$-based SCR-DeNOx catalyst was used as a support to synthesize $CeMn/SCR_1$ catalysts. The $Hg^0$ oxidation activities were tested at 100–300 °C in simulated coal-fired flue gas without HCl. The effects of Ce/Mn mass ratios, flue gas components including $NH_3$, $SO_2$, $H_2O$, and $O_2$ were evaluated. Besides, in order to further investigate the improvement of physicochemical properties by the modified Ce-Mn mixed oxide, Brunauer-Emmett-Teller (BET), scanning electron microscopy (SEM), X-ray diffractogram (XRD), and X-ray photoelectron spectroscopy (XPS) analyses were carried out and analyzed in detail. The catalytic mechanism for simultaneous removal of $Hg^0$ and NO was investigated in the end.

## Experimental

### The preparation of catalysts

The spent $TiO_2$-based SCR-DeNOx catalysts were obtained from power plant after exposure to exhaust gases in the SCR system for 3 years. Their $DeNO_x$ activity (about 30.00 %) was much less than fresh ones. The spent $TiO_2$-based SCR catalysts were washed in deionized water to remove poisons such as ash, alkali metals, and salt molecules from the samples. Once washing was completed, the sample was dried in an oven at 105 °C for 12 h. Finally, the samples were crushed and sieved to 100–120 mesh. The samples are denoted as $SCR_1$ catalysts and stored in desiccator.

The $Ce/SCR_1$, $Mn/SCR_1$, and $CeMn/SCR_1$ samples were prepared using cerium nitrate and/or manganese nitrate aqueous solution and $SCR_1$ catalysts by an impregnation method enhanced by ultrasound. Specifically as follows: first, a certain amount of cerium nitrate and/or manganese nitrate was dissolved in deionized water to form the solution. Then, the $SCR_1$ catalyst was added to the solution with stirring in a proportion. Third, the mixture was exposed to an ultrasonic bath for 1 h. Excess water was evaporated while stirring and ultrasonic bath. The obtained solid was dried at 105 °C for 12 h and calcined at 500 °C for 3 h. Finally, the obtained catalysts were ground and sieved to 100–120 mesh. The catalysts were denoted as $Mn/SCR_1$, $Ce/SCR_1$, and $Ce_xMn/SCR_1$, where x represented the Ce/Mn mass ratio (0.25,

0.67, 1.00, 1.50, and 4.00). The mass loading of ($CeO_2$+ $MnO_x$)/$SCR_1$ were 1 %. The mass loading of Ce/$SCR_1$ or Mn/$SCR_1$ were 1 % as well.

### Catalyst characterization

The analysis of surface area, average pore size, and average pore volume was carried by Micromeritics Tristar II 3020 analyzer (Micromeritics Instrument Crop, USA). All samples were degassed in vacuum at 180 °C for 5 h. The specific surface area was determined using the standard Brunauer-Emmett-Teller (BET) equation. The average pore diameter and average pore volume of the samples were obtained from the desorption branches of $N_2$ adsorption isotherm and calculated by the Barrett-Joyner-Halenda (BJH) formula.

To further analyze the morphology and surface structure of the samples, SEM analysis was performed using a Hitachi S-4800 (Hitachi Limited, Japan). The separated areas for each sample were magnified to ×100,000.

The samples were characterized by XRD using a Rigaku rotaflex D/Max-C powder diffractometer (Rigaku, Japan) with Cu-Ka radiation (l=1.5406 A°) in the 2$\theta$ range from 10° to 80° with 0.2°/min.

XPS experiments were performed on a K-Alpha 1063 X-ray photoelectron spectrometer (Thermo Fisher Scientific, UK). XPS spectra were obtained using an Al $K_a$ X-ray source operated at 12 kV and 6 mA. The observed spectra were calibrated with the carbon 1s electron binding energy (BE) value of 284.6 eV.

### Catalytic activity measurement

The experiments were performed in a fixed-bed quartz reactor (i.d. 20 mm), which was located inside a temperature-controlled tubular furnace, as shown in Fig. 1. An $Hg^0$ permeation tube (VICI Metronics, USA) was used to generate a constant quantity of $Hg^0$ vapor (70.00 μg/$m^3$), which was supplied into the gas steam. Other simulated flue gas (SFG) components including 300 ppm $SO_2$, 500 ppm NO, 500 ppm $NH_3$ (when used), 12 % $CO_2$, 8 % $H_2O$ vapor (when used), 5 % $O_2$, and balanced gas $N_2$ were supplied by gas cylinders and were precisely controlled by mass flow controllers (MFC). A total flow rate of 1 L/min were used during the experiments, which corresponded to a gas hourly space velocity (GHSV) of 100,000/h (the catalysts mass was 0.5 g). All the gas components were mixed and preheated to the desired temperature, and then passed through the fixed-bed quartz reactor. The feed water was exactly controlled by peristaltic pump and injected into the Teflon tube that wrapped with a temperature-controlled heating tape. Afterward, the water vapor was generated. One hundred milliliters per minute pure $N_2$ took along the water vapor to mix with the flue gas. Besides, in order to avoid adsorption of $Hg^0$ on the inner surface and condensation of water vapor, all Teflon tubes that $Hg^0$ and water vapor passed through were heated up to 120 °C. A RA-915M mercury analyzer (LUMEX Ltd, Russia) was employed to measure the concentration of $Hg^0$ while NO concentration was monitored by a flue gas analyzer (MGA5, Germany). It was verified that interferences on $Hg^0$ measurement by flue gas components such as $SO_2$, $NH_3$, and water vapor were negligible. Even so, before proceeding to the mercury analyzer, acid gases, $NH_3$, and water vapor were removed by the conditioning unit and the condenser. The conditioning unit converged to a 10 % NaOH solution in which gases such as $NH_3$ and $SO_2$ were captured. The $H_2O$ vapor condensed into liquid water through the condenser.

Six sets of experiments were conducted, and the experimental conditions are summarized in Table 1. In set I to set II, experiments aimed at finding the optimal catalyst and operating temperature. The $Hg^0$ oxidation activities over $SCR_1$, Mn/$SCR_1$, Ce/$SCR_1$, and $Ce_xMn/SCR_1$ samples were evaluated under SFG (500 ppm NO, 300 ppm $SO_2$, 5 % $O_2$, 12 % $CO_2$, and 70.00 μg/$m^3$ $Hg^0$) for 2 h. In set III to set V, the effects of individual gas components on $Hg^0$ oxidation and the reaction pathways were explored. The experiments were conducted on the optimal sample in the presence of individual flue gases at optimal operating temperature. In set VI, the optimal sample was tested in SCR atmosphere (500 ppm NO, 500 ppm $NH_3$, 300 ppm $SO_2$, 5 % $O_2$, and 70.00 μg/$m^3$ $Hg^0$) at each selected reaction temperature from 100 to 300 °C for investigating the simultaneous removal of $NO_x$ and $Hg^0$.

At the beginning of each test for catalytic activity, the gas stream bypassed the reactor and the inlet gas was sampled to ensure a stable NO ($NO_{in}$) and $Hg^0$ ($Hg^0_{in}$) feed concentration. Then, the gas flow was switched to pass through the catalysts, and the analyzer measured the gas compositions in the outlet (noted as $NO_{out}$ and $Hg^0_{out}$). Before each test, the catalysts were first saturated with the established $Hg^0_{in}$ under $N_2$ atmosphere at room temperature to avoid possible bias because of $Hg^0$ physical adsorption (Anchao et al. 2014; Li et al. 2012; Li et al. 2011). The result indicated that $Hg^0$ physical adsorption capacity of samples were negligible at room temperature (less than 1.0 μg/g at room temperature). Therefore, the loss of $Hg^0$ over the catalysts should be due to the oxidation of $Hg^0$. $Hg^0$ oxidation efficiency ($\eta_{Hg}$) over the catalysts was quantified by Eq. (1):

$$\eta_{Hg}(\%) = \frac{Hg^0_{in} - Hg^0_{out}}{Hg^0_{in}} \times 100\% \quad (1)$$

Meanwhile, the NO conversion efficiency ($\eta_{NO}$) can be calculated using Eq. (2):

$$\eta_{NO}(\%) = \frac{NO_{in} - NO_{out}}{NO_{in}} \times 100\% \quad (2)$$

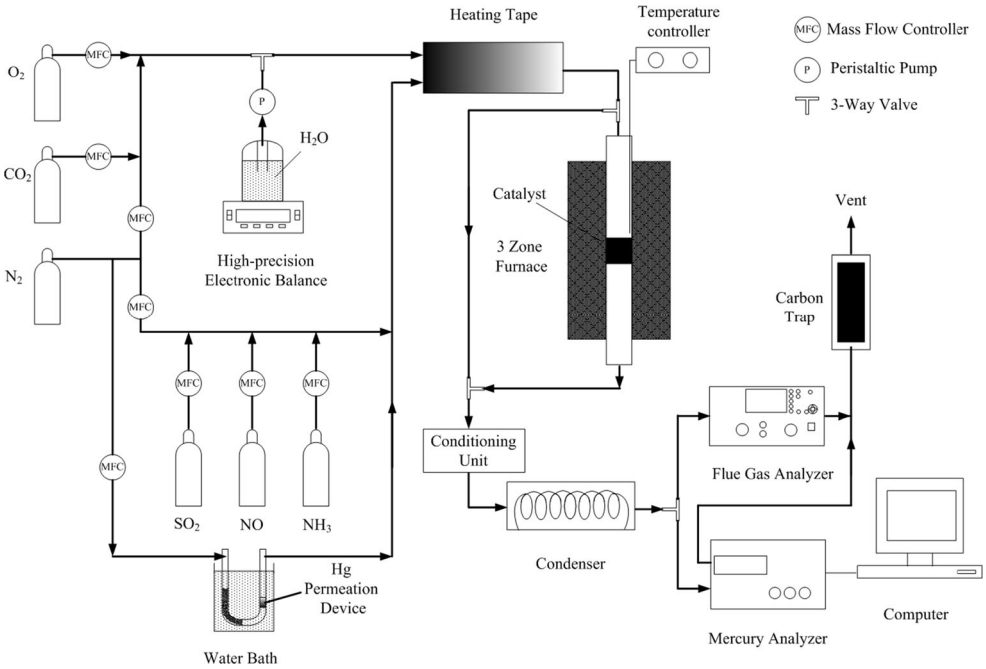


**Fig. 1** Schematic diagram of the experimental setup

## Results and discussion

### Characterization of the catalyst

*BET*

The BET specific surface area, pore volumes, and average pore sizes of the samples are listed in Table 2. Compared to the $SCR_1$ catalyst, the addition of Mn reduced the surface areas of catalysts. The reason might be that $MnO_x$ occupied a part of free pores of supports during the impregnation process. Note that the surface areas of the sample were increased after the addition of Ce. This result suggested that Ce could improve the specific surface areas of catalysts. However, the BET surface areas of all samples had no obvious change. Furthermore, pore volumes of $Ce_{1.00}Mn/SCR_1$ catalyst were lower than that of $Mn/SCR_1$ and $Ce/SCR_1$. It has been reported that a prominent synergy effect could be exhibited between $CeO_2$ and $MnO_x$ (Singh et al. 2013).

**Table 1** Experimental conditions

| Experiments | Catalysts | Flue gas components(1 L/min) | Temperature (°C) |
|---|---|---|---|
| Set I | $SCR_1$, $Ce/SCR_1$, $Mn/SCR_1$, $Ce_{1.00}Mn/SCR_1$ | $N_2$+70.00 μg/m$^3$ $Hg^0$+500 ppm NO+300 ppm $SO_2$+ 12 % $CO_2$+5 % $O_2$ | 100–300 |
| Set II | $Ce_xMn/SCR_1$ | $N_2$+70.00 μg/m$^3$ $Hg^0$+500 ppm NO+300 ppm $SO_2$+ 12 % $CO_2$+5 % $O_2$ | 100–200 |
| | $SCR_1$, $Ce/SCR_1$ | $N_2$+70.00 μg/m$^3$ $Hg^0$ | |
| Set III | $Mn/SCR_1$, $Ce_{1.00}Mn/SCR_1$ | $N_2$+70.00 μg/m$^3$ $Hg^0$+500 ppm $NH_3$, $N_2$+70.00 μg/m$^3$ $Hg^0$+ 500 ppm $NH_3$+5 % $O_2$, $N_2$+70.00 μg/m$^3$ $Hg^0$+500 ppm $NH_3$+ 500 ppm NO+5 % $O_2$, $N_2$+70.00 μg/m$^3$ $Hg^0$+400 ppm $NH_3$+ 500 ppm NO+5 % $O_2$ | The optimal reaction temperature |
| Set IV | $Ce_{1.00}Mn/SCR_1$ | $N_2$+70.00 μg/m$^3$ $Hg^0$+0–1000 ppm $SO_2$+5 % $O_2$, $N_2$+ 70.00 μg/m$^3$ $Hg^0$+0–1000 ppm $SO_2$, $N_2$+70.00 μg/m$^3$ $Hg^0$+ 600 ppm $SO_2$+5 % $O_2$, $N_2$+70.00 μg/m$^3$ $Hg^0$+600 ppm $SO_2$, $N_2$+ 70.00 μg/m$^3$ $Hg^0$+5 % $O_2$+8 % $H_2O$+300 ppm $SO_2$ | 150 |
| Set V | $Ce_{1.00}Mn/SCR_1$ | $N_2$+70.00 μg/m$^3$ $Hg^0$+0–10 % $O_2$+100 ppm $NH_3$+100 ppm NO | 150 |
| Set VI | $Ce_{1.00}Mn/SCR_1$ | $N_2$+70.00 μg/m$^3$ $Hg^0$+500 ppm NO+500 ppm $NH_3$+300 ppm $SO_2$+5 % $O_2$ | 100–300 |

**Table 2** The surface area, pore volume, and pore diameter of the samples

| Catalysts | BET surface area ($m^2$/g) | Pore volume ($cm^3$/g) | Average pore diameter (nm) |
|---|---|---|---|
| $SCR_1$ | 42.3059 | 0.1872 | 17.7077 |
| Ce /$SCR_1$ | 43.1618 | 0.1860 | 13.7511 |
| Mn/$SCR_1$ | 41.7101 | 0.1816 | 17.4146 |
| $Ce_{1.00}Mn/SCR_1$ | 42.0066 | 0.1355 | 12.9051 |

Therefore, it could be inferred that the loss of pore volumes might be caused by deposited Ce-Mn mixed-oxide, which penetrated into the pores of carriers.

*SEM*

The SEM images of the selective samples are shown in Fig. 2. The SEM images showed that crystal morphologies of the $SCR_1$ catalyst were not significant influenced by the addition of metal oxide. From Fig. 2a, it could be seen that the surface of $SCR_1$ catalyst was smooth and the size was uniform. For Ce/$SCR_1$ or Mn/$SCR_1$ catalyst, a few depositions of $CeO_2$ or $MnO_x$ formed, while on the $Ce_{1.00}Mn/SCR_1$ catalyst surface (Fig. 2d), more depositions were observed. Since the BET surface areas had no significant change as demonstrated in Table 2, it can be concluded that the dispersion of $CeO_2$ or $MnO_x$ on the support surface was excellent. However, a synergy effect between $CeO_2$ and $MnO_x$ could result in particles interconnection, which promoted the formation of agglomerates.

*XRD*

The XRD patterns of spent $SCR_1$, Ce/$SCR_1$, Mn/$SCR_1$, and $Ce_{1.00}Mn/SCR_1$ catalysts are shown in Fig. 3. It was found that the major reflections of XRD patterns belonged to anatase phase $TiO_2$. The addition of $CeO_2$ or/and $MnO_x$ did not result in significant change in the positions or the shapes of typical $TiO_2$ diffractions. Besides, for all the samples, no obvious traces of $CeO_2$ or/and $MnO_x$ were found in any of the catalysts during XRD analysis, which indicated that $CeO_2$ or/and $MnO_x$ species were well dispersed throughout the support structure or their crystalline structures were too small to detect.

*XPS*

To gain more insight into the reaction pathways, an XPS analysis was performed to determine the chemical state and the relative proportion of the elements on the surface of the fresh and spent $Ce_{1.00}Mn/SCR_1$ catalyst. The spent $Ce_{1.00}Mn/SCR_1$ catalysts were carried out on the fix bed reaction system under

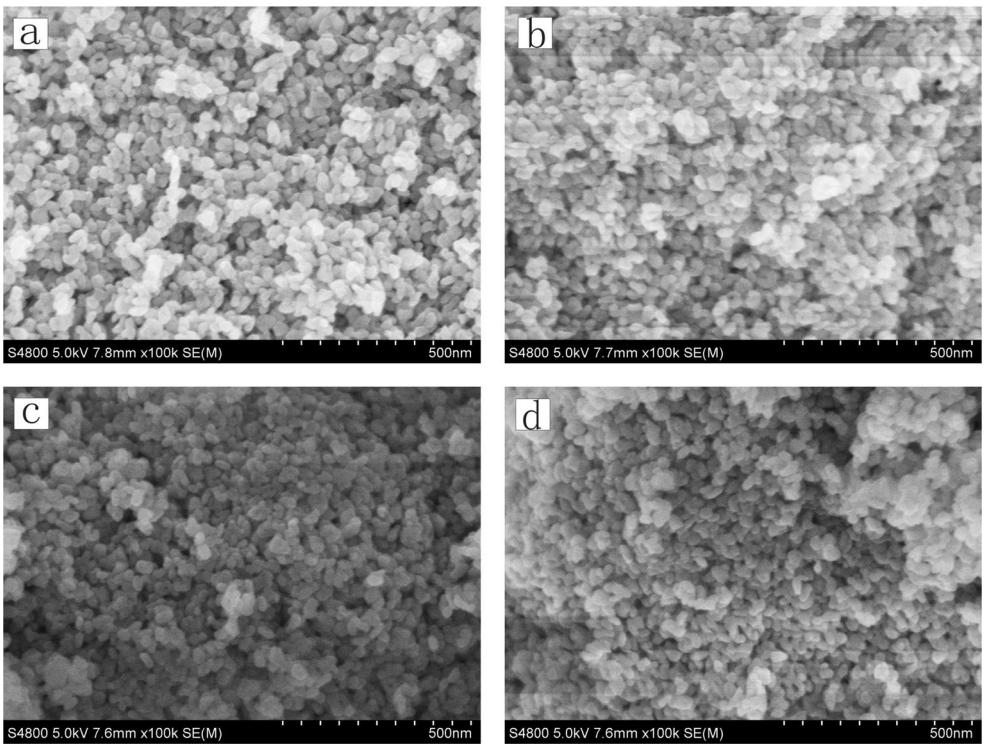


**Fig. 2** Nanoscale of SEM analysis of **a** $SCR_1$, **b** Ce/$SCR_1$, **c** Mn/$SCR_1$, **d** $Ce_{1.00}Mn/SCR_1$ (100,000 multiplier)

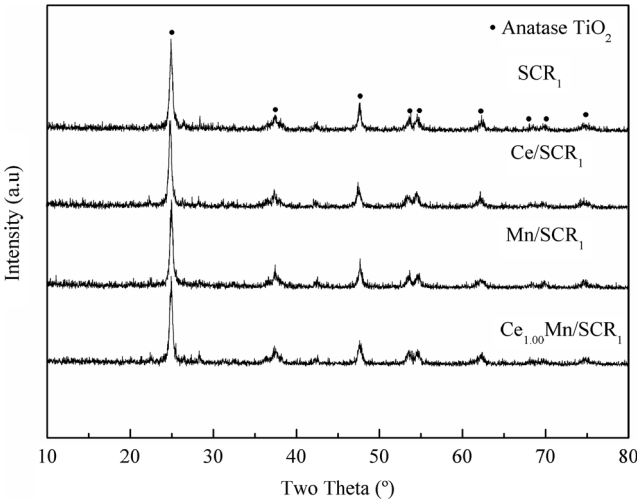


**Fig. 3** XRD patterns of $SCR_1$, $Ce/SCR_1$, $Mn/SCR_1$, and $Ce_{1.00}Mn/SCR_1$

SCR atmosphere at 150 °C. The XPS results are shown in Fig. 4. The O1s peaks could be fitted into two peaks referred to the lattice oxygen ($O_\beta$) at 529.3–530.0 eV and the chemisorbed oxygen ($O_\alpha$) at 531.3–531.9 eV (Wu et al. 2008). As shown in Fig. 4a, the $O_\beta$ ratio for the peak at 530.0 eV (calculated by $O_\beta/(O_\alpha+O_\beta)$) increased from 61.45 to 62.61 % compared to that of the fresh catalyst, whereas the ratio of $O_\alpha$ (calculated by $O_\alpha/(O_\alpha+O_\beta)$) decreased from 38.54 to 37.38 %. These observations suggested that both chemisorbed oxygen and lattice oxygen participated in $Hg^0$ oxidation and NO conversion. The increase of the $O_\beta$ ratio can be explained by two factors. First, $O_2$ in flue gas could regenerate the lattice oxygen which consumed in the reaction. Second, the consumption of chemisorbed oxygen increased the percentage of lattice oxygen.

The XPS spectra for Ce 3d are shown in Fig. 4b. XPS peaks denoted as u/v, $u_2/v_2$, and $u_3/v_3$ can be assigned to $Ce^{4+}$ while $u_1/v_1$ correspond to $Ce^{3+}$ (Wang et al. 2014). Both $Ce^{3+}$ and $Ce^{4+}$ existed in the fresh $Ce_{1.00}Mn/SCR_1$ catalyst. Based on the peak areas, the peaks corresponding to $Ce^{4+}$ appeared to be dominant. After the reaction, the ratio of $Ce^{4+}/Ce^{3+}$ decreased from 2.70 to 1.54 compared to the fresh catalyst, implying a reduction of $Ce^{4+}$ during the reaction. Furthermore, the presence of $Ce^{3+}$ may result in a charge imbalance, which would lead to oxygen vacancies and unsaturated chemical bonds (Liu et al. 2012). This situation could generate additional chemisorbed oxygen or weakly adsorbed oxygen species on the surface of the catalyst, which is beneficial for $Hg^0$ oxidation and the SCR reaction.

The XPS results of Mn 2p for the fresh and spent $Ce_{1.00}Mn/SCR_1$ catalyst are shown in Fig. 4c. For the fresh $Ce_{1.00}Mn/SCR_1$ catalyst, the peaks observed at 643.1 and 641.5 eV correspond to $Mn^{4+}$ and $Mn^{3+}$, respectively (Xu et al. 2012). The co-existence state of $MnO_2$–$Mn_2O_3$ can promote the catalytic oxidation activity of catalyst (Xu et al. 2012). For the catalyst

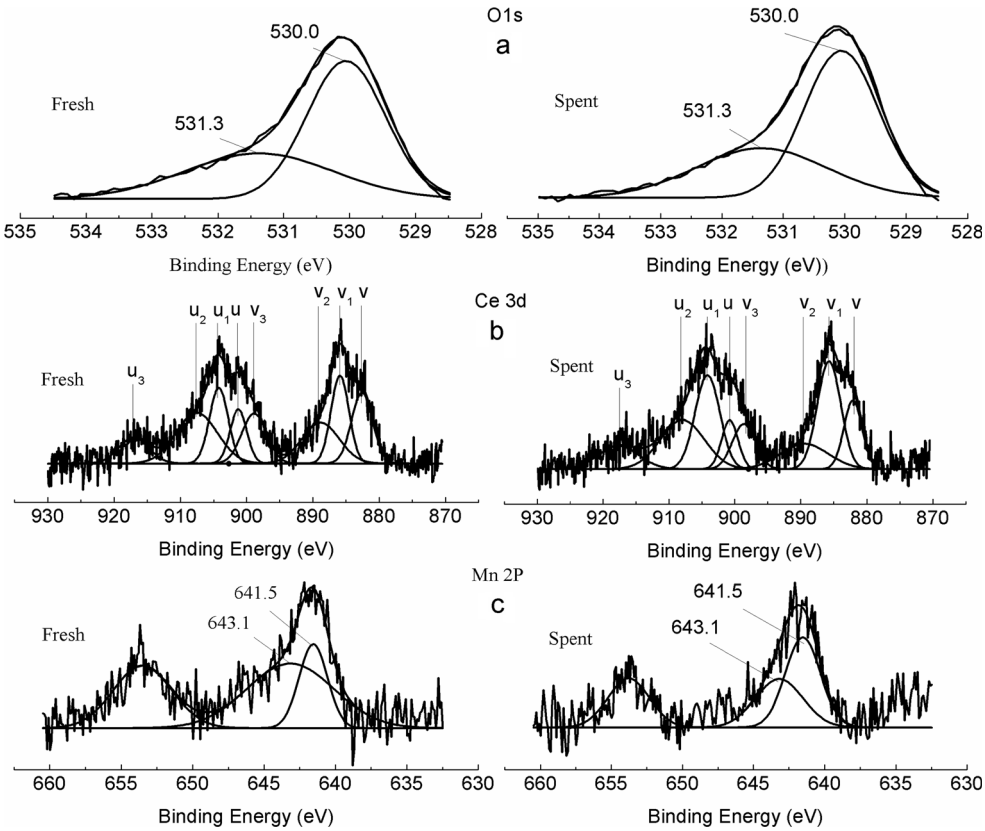


**Fig. 4** XPS spectra of $Ce_{1.00}Mn/SCR_1$ over the spectral regions of **a** O 1s, **b** Ce 3d, and **c** Mn 2p (reaction condition: 70.00 μg/m$^3$ $Hg^0$, 500 ppm NO, $NH_3$/NO: 1, 5 % $O_2$, 300 ppm $SO_2$, 500 mg of sample, 1000 mL/min total flow rate, and GHSV 100,000/h)

used at 150 °C, the ratio of $Mn^{4+}/Mn^{3+}$ decreased from 2.38 to 0.72. The result confirmed that reactions took place between the adsorbed active species and lattice oxygen (Wang et al. 2014). The lattice oxygen came from the valence state changes of $MnO_x$. $O_2$ in the flue gas would supply the metal oxide with oxygen to ensure that reaction can be continued. Therefore, it can be concluded that the lattice and chemisorbed oxygen on the catalyst surface are responsible for their superior performance. The reduction of $Mn^{4+}$ to $Mn^{3+}$ on the surface of the catalyst contributed to the $Hg^0$ oxidation.

## Performance of catalysts

### *Catalytic activity tests*

The activity curves of the different catalysts under simulated flue gas are shown in Fig. 5. Apparently, with the addition of $CeO_2$ or/and $MnO_x$ into $SCR_1$, the catalytic activity was obviously enhanced, especially at low temperature. Notably, $E_{oxi}$ over $Ce_{1.00}Mn/SCR_1$ catalyst was higher than that over $Mn/SCR_1$ and $Ce/SCR_1$ catalysts. This result demonstrated that there were intense interactions between manganese oxides and cerium oxides (Li et al. 2012). The interactions resulted in more surface oxygen, which is responsible for $Hg^0$ oxidation.

The $Hg^0$ oxidation of the $Ce_{1.00}Mn/SCR_1$ catalysts with different Ce/Mn mass ratios is shown in Fig. 6. According to the results of $Ce_{1.00}Mn/SCR_1$ catalysts, it can be seen that the $\eta_{Hg}$ first increased with the increasing of Ce/Mn mass ratios, then the $\eta_{Hg}$ decreased when the Ce/Mn mass ratios was 1.50. Remarkably, $Ce_{1.00}Mn/SCR_1$ catalyst showed the best activity, and its $Hg^0$ oxidation efficiency was 92.80 % at 150 °C. These results indicated that Ce/Mn mass ratios influenced the activity of $Ce_xMn/SCR_1$ catalysts, which is related to the synergy between $CeO_2$ and $MnO_x$.

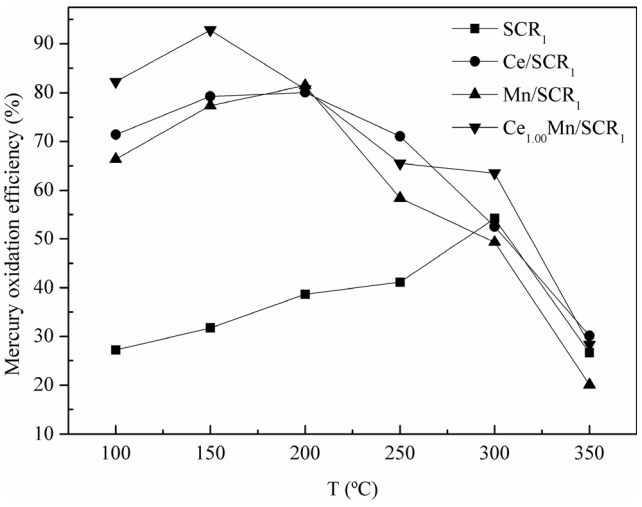


**Fig. 5** $Hg^0$ oxidation efficiency over different catalysts under simulated flue gas as a function of temperature (reaction condition: 70.00 μg/m$^3$ $Hg^0$, 500 ppm NO, 5 % $O_2$, 300 ppm $SO_2$, 12 % $CO_2$, 500 mg of sample, 100-300 °C, 1000 mL/min total flow rate, and GHSV 100,000/h)

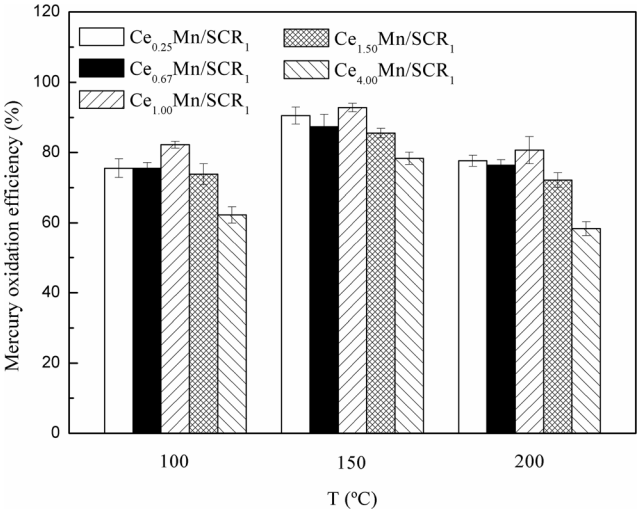


**Fig. 6** Effects of different of Ce/Mn mass ratio on $Ce_{1.00}Mn/SCR_1$ catalysts on $Hg^0$ oxidation efficiency (reaction condition: 70.00 μg/m$^3$ $Hg^0$, 500 ppm NO, 5 % $O_2$, 300 ppm $SO_2$, 12 % $CO_2$, 500 mg of sample, 100–200 °C, 1000 mL/min total flow rate, and GHSV 100,000/h)

### *Effect of $NH_3$ on $Hg^0$ oxidation*

Since $NH_3$ is the reactant gas for selective catalytic reduction of $NO_x$, it is necessary to study the effect of $NH_3$ on $Hg^0$ oxidation. Figure 7 shows the influence of $NH_3$ on mercury oxidation over $Ce_{1.00}Mn/SCR_1$ catalysts. In this work, a significant inhibitive effect of $NH_3$ on $Hg^0$ oxidation over the catalysts was observed both in pure $N_2$ atmosphere and in the presence of $O_2$. $NH_3$ (500 ppm) was added to pure $N_2$ atmosphere and gas flow containing 5 % $O_2$ balanced in $N_2$, respectively. It was observed that the $Hg^0$ oxidation efficiency

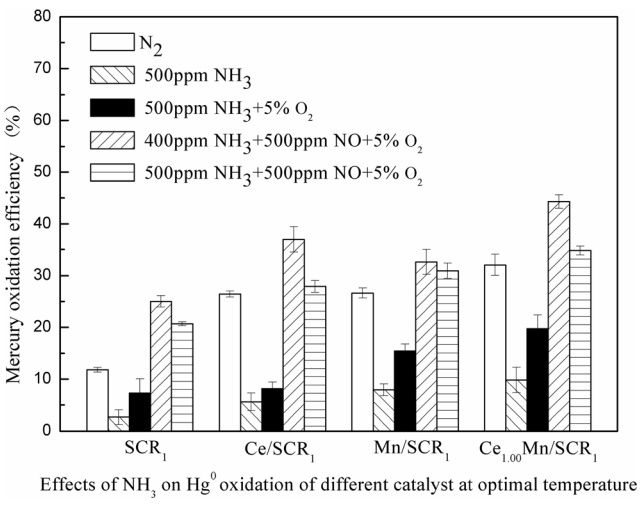


**Fig. 7** Effect of $NH_3$ on $Hg^0$ oxidation over different catalysts (reaction condition: 70.00 μg/m$^3$ $Hg^0$, 500 ppm $NH_3$, $NH_3$/NO: 0–1, 5 % $O_2$, the optimal reaction temperature, 500 mg of sample, 1000 mL/min total flow rate, and GHSV 100,000/h)

decreased. In the presence of $O_2$, $Hg^0$ oxidation dropped to only 19.73 % over $Ce_{1.00}Mn/SCR_1$ catalyst, which, however, was still higher than that without $O_2$. Some researchers believe that $NH_3$ adsorption on catalyst most probably takes place according to the following steps (Qi et al. 2004; Zhou et al. 2013):

$$NH_3(g) \rightarrow NH_3(ad) \quad (3)$$

$$NH_3(ad) + O^*(ad) \rightarrow NH_2(ad) + OH(ad) \quad (4)$$

where O* are active surface oxygen of the catalyst. In this process, $NH_3$ consumed the surface oxygen (including lattice oxygen and chemisorbed oxygen) that is responsible for $Hg^0$ oxidation and NO conversation. Gas-phase $O_2$ regenerated the lattice oxygen, and replenished the consumed chemisorbed oxygen. Thus, the presence of gas-phase $O_2$ offsets part of the inhibitive effect of $NH_3$. Interestingly, the coexistence of NO with $NH_3$ can also mitigate such inhibition. $\eta_{Hg}$ was 34.79 % in $N_2$+500 ppm NO+500 ppm $NH_3$+5 %$O_2$, which was higher than that in $N_2$+500 ppm $NH_3$. In addition, the $\eta_{Hg}$ over $Ce_{1.00}Mn/SCR$ catalyst was also higher than that of $SCR_1$ catalyst. It indicated the participation of $CeO_2$ and $MnO_x$ had certain effects on reducing the inhibitive effect of $NH_3$.

### *Effect of $SO_2$ and $H_2O$ on $Hg^0$ oxidation*

It is very important to evaluate the effect of $SO_2$ and $H_2O$ on $Hg^0$ oxidation because $SO_2$ and $H_2O$ unavoidably exist in flue gas and have significant impacts on the activities of catalysts. Figure 8 presents the effects of $SO_2$ and $H_2O$ on $Hg^0$ oxidation over $Ce_{1.00}Mn/SCR_1$ catalysts at 150 °C. It can be seen that $Hg^0$ oxidation was not promoted by $SO_2$ itself. Otherwise, $Hg^0$ oxidation efficiency should not rely on the existence of $O_2$ and should rise with the increase of $SO_2$ concentration (Li et al. 2013). As shown in Fig. 8a, introducing 200 ppm $SO_2$ into gas flow containing 5 % $O_2$ increased $Hg^0$ oxidation efficiency from 60.15 to 63.10 %, which indicated that low $SO_2$ concentration promoted $Hg^0$ oxidation with the aid of $O_2$. However, $Hg^0$ oxidation efficiency gradually decreased as $SO_2$ concentration increased from 200 to 1000 ppm. As can be seen in Fig. 8a (inset), $\eta_{Hg}$ maintained at almost the same level throughout the entire experimental period with the aid of $O_2$. However, without the aid of $O_2$, the $Hg^0$ oxidation efficiency was influenced with a drop of 34.56 %, and a continuous declining trend was observed as time went by. It demonstrated that part of adsorbed $SO_2$ reacted with catalyst to form some new species that were responsible for the enhanced $Hg^0$ oxidation. For metal-oxide-based SCR catalysts, the new species was generally believed to be $SO_3$ (Casapu et al. 2009; Dunn et al. 1998; Fan et al. 2010; Svachula et al. 1993). Therefore, it was inferred that $SO_2$ would be oxidized by the lattice oxygen, reducing the active oxidant sites. The reduced

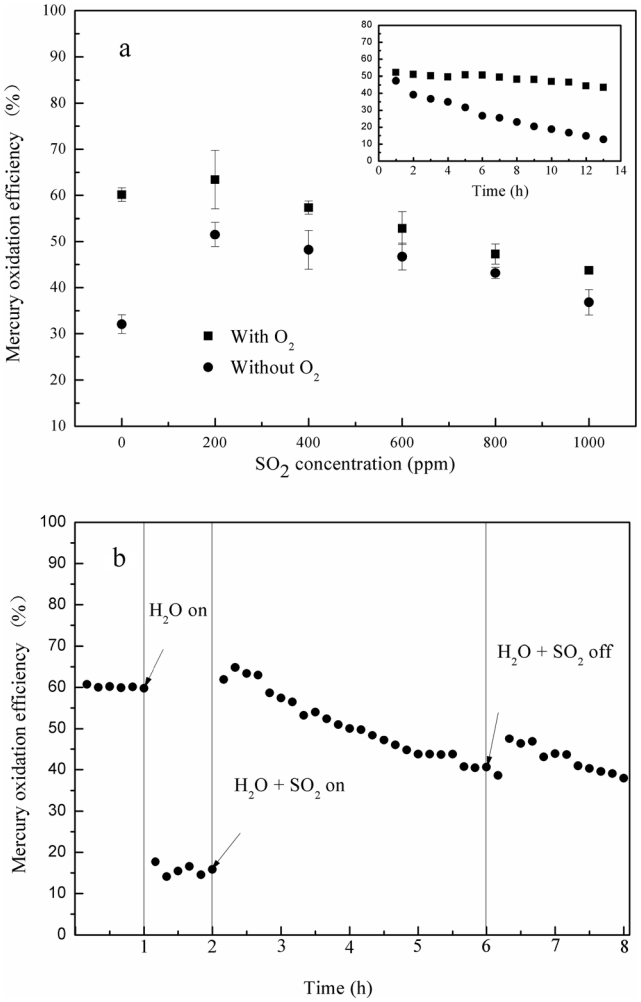


**Fig. 8** Effect of $SO_2$ and $H_2O$ on $Hg^0$ oxidation over $Ce_{1.00}Mn/SCR_1$ catalysts. **a** Effect of $SO_2$ concentration on $Hg^0$ oxidation (reaction condition: 70.00 μg/m$^3$ $Hg^0$, 0–1000 ppm $SO_2$, 5 % $O_2$, 500 mg of sample, 150 °C, 1000 mL/min total flow rate, and GHSV 100,000/h). **b** Effect of $SO_2$ and $H_2O$ on $Hg^0$ oxidation (reaction condition: 70.00 μg/m$^3$ $Hg^0$, 300 ppm $SO_2$, 8 % $H_2O$, 5 % $O_2$, 500 mg of sample, 150 °C, 1000 mL/min total flow rate, and GHSV 100,000/h)

active sites could not be reactivated without $O_2$, which resulted in the decrease of $Hg^0$ oxidation efficiency as time went by. On the other hand, with the aid of $O_2$, the reduced oxidant sites were reoxidized by $O_2$. Both the reactivated sites and $SO_3$ promoted $Hg^0$ oxidation efficiency. A promotional effect of $SO_2$ on $Hg^0$ oxidation can be proposed as follows (Li et al. 2008a):

$$SO_2 + \frac{1}{2}O_2 \rightarrow SO_3 \quad (5)$$

$$Hg^0 + \frac{1}{2}O_2 + SO_3 \rightarrow HgSO_4 \quad (6)$$

Figure 8b illustrates the activity performance of $Ce_{1.00}Mn/SCR_1$ catalysts in the system with $SO_2$ and water vapor simultaneously. As is shown, when adding 8 % $H_2O$ into the stream,

the $Hg^0$ oxidation efficiency dropped sharply. Obviously, $H_2O$ had a significant inhibitive effect on $Hg^0$ oxidation (Li et al. 2008b). The inhibitive effect of $H_2O$ possibly came from its competitive occupancy of the available active sites and displacement of adsorbed $Hg^0$ (Tan et al. 2012). When both $H_2O$ and $SO_2$ were added, the inhibition was less severe than that when $H_2O$ were added individually. This indicates that $H_2SO_4$ can form when $SO_2$, $O_2$, and $H_2O$ co-exist, which will likely affect the behavior of $Hg^0$ on the surface of catalyst. After the $H_2O$ and $SO_2$ were cut off, it was found that the catalytic activity gradually recovered but not returned to the original level yet. It implies that the addition of $SO_2$ can reduce the $H_2O$ poison. However, the catalysts were deactivated by $H_2SO_4$ somehow.

### *Effect of $O_2$*

To obtain higher catalytic oxidation, the presence of $O_2$ is normally necessary, especially for metal oxide catalysts (Anchao et al. 2014). Figure 9 shows the effect of $O_2$ on catalytic activity of $Ce_{1.00}Mn/SCR_1$ catalysts. The results showed that the NO conversion and $Hg^0$ oxidation efficiency in $N_2$+2 % $O_2$ was greater than that in pure $N_2$ atmosphere. This observation indicated that $O_2$ is beneficial to the catalytic activity of catalyst. Meanwhile, $Hg^0$ oxidation might comprise some chemical reactions with the presence of $O_2$ (Fan et al. 2012; Tao et al. 2012; Yang et al. 2011a; Yang et al. 2011b). Combined with the XPS results, it was possible that gas-phase $O_2$ achieved the supplement of the lost lattice oxygen, which facilitated $Hg^0$ oxidation and NO conversion.

### *Simultaneous removal of $Hg^0$ and NO*

The simultaneous removal of $Hg^0$ and NO by $Ce_{1.00}Mn/SCR_1$ catalysts was also investigated and the results are illustrated in Fig. 10. As shown in the figure, 82.20 % NO conversion was obtained at 200 °C with a GHSV of 100,000/h. An obvious decrease of the $Hg^0$ oxidation efficiency was found in the experiment compared with the $NH_3$-free condition. Although simultaneously removal of $Hg^0$ and NO was unsatisfactory, it is still encouraging because lower space velocity would result in higher $Hg^0$ oxidation efficiency and NO conversion. Combined with the result of upper experiment, the problem that how to design and choose the best optimized experimental conditions for simultaneous removal of $Hg^0$ and NO still needs further study.

## The cooperation of Mn and Ce in the SCR catalysts

It was worthy noted that the reaction on the surface of $Ce_{1.00}Mn/SCR_1$ catalysts included both NO conversion and $Hg^0$ oxidation. NO was reduced by $NH_3$ through the catalysis of $NH_3$-SCR while $Hg^0$ was oxidized to $Hg^{2+}$. The reaction observed in this work like previous literature (He et al. 2014; Singh et al. 2013; Xu et al. 2012) which is thought to be aided by the synergistic mechanism between the manganese and cerium oxides. They explained the synergistic mechanism as follows:

$$2MnO_2 \rightarrow Mn_2O_3 + O_\beta \quad (7)$$

$$Mn_2O_3 + 2CeO_2 \rightarrow 2MnO_2 + Ce_2O_3 \quad (8)$$

$$Ce_2O_3 + \frac{1}{2}O_2 \rightarrow 2CeO_2 \quad (9)$$

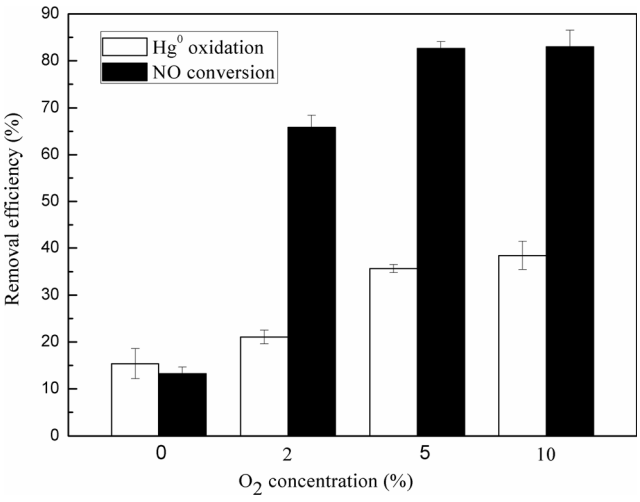


**Fig. 9** Effect of $O_2$ concentration on simultaneous removal of $Hg^0$ and NO over $Ce_{1.00}Mn/SCR_1$ catalysts at 150 °C (reaction condition: 70.00 μg/m$^3$ $Hg^0$, 100 ppm NO, $NH_3$/NO: 1, 0–10 % $O_2$, 500 mg of sample, 150 °C, 1000 mL/min total flow rate, and GHSV 100,000/h)

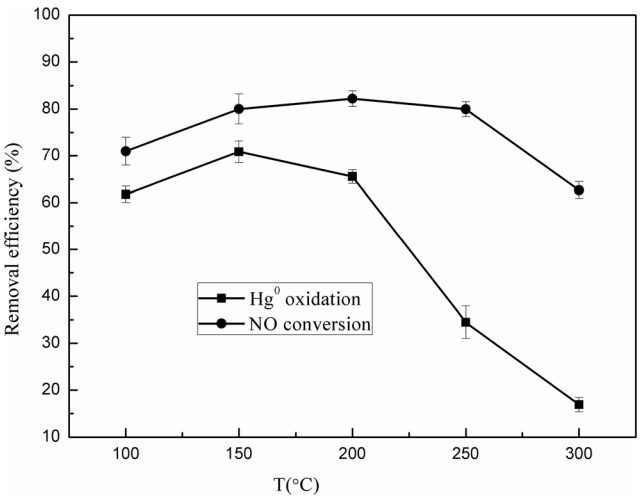


**Fig. 10** $Hg^0$ oxidation and NO conversion with respect to reaction temperatures (reaction condition: 70.00 μg/m$^3$ $Hg^0$, 500 ppm NO, $NH_3$/NO: 1, 300 ppm $SO_2$, 5 % $O_2$, 500 mg of sample, 100–300 °C, 1000 mL/min total flow rate, and GHSV 100,000/h)

The co-existence of $MnO_2$-$Mn_2O_3$ can improve the NO conversion and $Hg^0$ oxidation. The lattice oxygen generated from manganese oxides are beneficial in promoting the oxygen cycle. Moreover, the additional oxygen generated is thought to be aided by the oxygen transfer between $Mn_2O_3$ and $CeO_2$ (Eq. 8). Ce provided oxygen to Mn, in which why the valence and oxidation ability of Mn increased. Finally, the consumed lattice oxygen would be replenished by oxygen from the flue gas (Eq. 9).

Combining with our results, the lattice oxygen participated in the NO conversion and $Hg^0$ oxidation. On one hand, the lattice oxygen generated via Eq. 10 is invariably responsible for the oxidation of NO to the intermediate $NO_2$-containing species on the catalyst surface. They can further react with $NH_3$ to form ammonium nitrite ($NH_2NO$), which subsequently decomposes into $N_2$ and $H_2O$. The reaction pathway can be described by Eqs. 10–12 according to the previous study (Jin et al. 2010). On the other hand, $Hg^0_{(ad)}$ would react with lattice oxygen that replenished by oxygen from the flue gas to form HgO. The pathway could be explained by Eqs. 13 and 14 according to the previous research (Ji et al. 2008; Kong et al. 2011; Zhao et al. 2014).

$$NO + O_\beta \rightarrow \cdots\cdots -O-N-O \quad (10)$$

$$\cdots\cdots -O-N-O + NH_3 + H^+ \rightarrow NH_4NO_2 \quad (11)$$

$$NH_4NO_2 \rightarrow NH_2NO \rightarrow N_2 + H_2O \quad (12)$$

$$Hg^0_{(g)} \rightarrow Hg^0_{(ad)} \quad (13)$$

$$Hg^0_{(ad)} + O_\beta \rightarrow HgO \quad (14)$$

where $\cdots\cdots$ represent the catalyst surface.

## Conclusions

The spent $TiO_2$-based SCR-DeNOx catalyst was used as a support for $Hg^0$ oxidation, which presents a more environmentally and financially sound option for simultaneous removal of $Hg^0$ and NO in industrial application. Ce-Mn mixed oxide modified catalyst was highly active for $Hg^0$ oxidation reaction at low temperature. The $Ce_{1.00}Mn/SCR_1$ catalyst exhibited high $Hg^0$ oxidation efficiency (92.80 %) at 150 °C. The flue gas components were found to have significant effects on Hg oxidation efficiency. $NH_3$ consumed the oxygen on the catalyst surface, hence inhibiting $Hg^0$ oxidation. Promotional effects of $SO_2$ on the $Hg^0$ oxidation were observed, while the presence of $H_2O$ inhibited the $Hg^0$ oxidation. Results also indicated that the combination of $CeO_2$ and $MnO_x$ resulted in significant synergy for $Hg^0$ oxidation and NO conversion.

**Acknowledgments** This project was financially supported by the National Natural Science Foundation of China (51278177, 51478173).

## References

Anchao Z, Wenwen Z, Jun S, Song H, Zhichao L, Jun X (2014) Cobalt manganese oxides modified titania catalysts for oxidation of elemental mercury at low flue gas temperature. Chem Eng J 236:29–38. doi:10.1016/j.cej.2013.09.060

Auzmendi-Murua I, Castillo Á, Bozzelli JW (2014) Mercury oxidation via chlorine, bromine, and iodine under atmospheric conditions: thermochemistry and kinetics. J Phy Chem A 118:2959–2975. doi:10.1021/jp412654s

Brown TD, Smith DN, Hargis RA, O'Dowd WJ (1999) Mercury measurement and its control: what we know, have learned, and need to further investigate. J Air Waste Manage Assoc 49:1–97. doi:10.1080/10473289.1999.10463906

Cao Y, Gao Z, Zhu J, Wang Q, Huang Y, Chiu C, Parker B, Chu P, Pan WP (2008) Impacts of halogen additions on mercury oxidation, in a slipstream selective catalyst reduction (SCR), reactor when burning sub-bituminous coal. Environ Sci Technol 42:256–261. doi:10.1021/es071281e

Casapu M, Kröcher O, Elsener M (2009) Screening of doped $MnO_x$–$CeO_2$ catalysts for low-temperature NO-SCR. Appl Catal B-Environ 88:413–419. doi:10.1016/j.apcatb.2008.10.014

Dunn JP, Koppula PR, Stenger HG, Wachs IE (1998) Oxidation of sulfur dioxide to sulfur trioxide over supported vanadia catalysts. Appl Catal B-Environ 19:103–117. doi:10.1016/S0926-3373(98)00060-5

Fan X, Li C, Zeng G, Gao Z, Chen L, Zhang W, Gao H (2010) Removal of gas-phase element mercury by activated carbon fiber impregnated with $CeO_2$. Energ Fuel 24:4250–4254. doi:10.1021/ef100377f

Fan X, Li C, Zeng G, Zhang X, Tao S, Lu P, Li S, Zhao Y (2012) The effects of Cu/HZSM-5 on combined removal of $Hg^0$ and NO from flue gas. Fuel Process Technol 104:325–331. doi:10.1016/j.fuproc.2012.06.003

Guo Y, Liu Z, Liu Q, Huang Z (2008) Regeneration of a vanadium pentoxide supported activated coke catalyst-sorbent used in simultaneous sulfur dioxide and nitric oxide removal from flue gas: effect of ammonia. Catal Today 131:322–329. doi:10.1016/j.cattod.2007.10.032

He J, Reddy GK, Thiel SW, Smirniotis PG, Pinto NG (2013) Simultaneous removal of elemental mercury and NO from flue gas using CeO2 modified MnOx/TiO2 materials. Energ Fuel 27:4832–4839. doi:10.1021/ef400718n

He C, Shen B, Chen J, Cai J (2014) Adsorption and oxidation of elemental mercury over Ce-MnOx/Ti-PILCs. Environ Sci Technol 48:7891–7898. doi:10.1021/es5007719

Ji L, Sreekanth PM, Smirniotis PG, Thiel SW, Pinto NG (2008) Manganese oxide/titania materials for removal of NOx and elemental mercury from flue gas. Energ Fuel 22:2299–2306. doi:10.1021/ef700533q

Jin R, Liu Y, Wu Z, Wang H, Gu T (2010) Low-temperature selective catalytic reduction of NO with $NH_3$ over MnCe oxides supported on $TiO_2$ and $Al_2O_3$: a comparative study. Chemosphere 78:1160–1166. doi:10.1016/j.chemosphere.2009.11.049

Kamata H, Ueno S, Naito T, Yukimura A (2008) Mercury oxidation over the $V_2O_5(WO_3)/TiO_2$ commercial SCR catalyst. Ind Eng Chem Res 47:8136–8141. doi:10.1021/ie800363g

Khodayari R, Odenbrand CUI (2001) Regeneration of commercial $TiO_2$-$V_2O_5$-$WO_3$ SCR catalysts used in bio fuel plants. Appl Catal B-Environ 30:87–99. doi:10.1016/S0926-3373(00)00227-7

Kong F, Qiu J, Liu H, Zhao R, Ai Z (2011) Catalytic oxidation of gas-phase elemental mercury by nano-$Fe_2O_3$. J Environ Sci 23:699–704. doi:10.1016/S1001-0742(10)60438-X

Larachi F, Pierre J, Adnot A, Bernis A (2002) Ce 3d XPS study of composite $Ce_xMn_{1-x}O_{2-y}$ wet oxidation catalysts. Appl Surf Sci 195:236–250. doi:10.1016/S0169-4332(02)00559-7

Li Y, Murphy P, Wua CY (2008a) Removal of elemental mercury from simulated coal-combustion flue gas using a $SiO_2$-$TiO_2$ nanocomposite. Fuel Process Technol 89:567–573. doi:10.1016/j.fuproc.2007.10.009

Li Y, Murphy PD, Wu CY, Powers KW, Bonzongo JCJ (2008b) Development of silica/vanadia/titania catalysts for removal of elemental mercury from coal-combustion flue gas. Environ Sci Technol 42:5304–5309. doi:10.1021/es8000272

Li JF, Yan NQ, Qu Z, Qiao SH, Yang SJ, Guo YF, Liu P, Jia JP (2010) Catalytic oxidation of elemental mercury over the modified catalyst Mn/alpha-$Al_2O_3$ at lower temperatures. Environ Sci Technol 44:426–431. doi:10.1021/es9021206

Li HL, Wu CY, Li Y, Zhang JY (2011) CeO2-TiO2 catalysts for catalytic oxidation of elemental mercury in low-rank coal combustion flue Gas. Environ Sci Technol 45:7394–7400. doi:10.1021/es2007808

Li H, Wu CY, Li Y, Zhang J (2012) Superior activity of $MnO_x$-$CeO_2$/$TiO_2$ catalyst for catalytic oxidation of elemental mercury at low flue gas temperatures. Appl Catal B-Environ 111–112:381–388. doi:10.1016/j.apcatb.2011.10.021

Li H, Wu CY, Li Y, Li L, Zhao Y, Zhang J (2013) Impact of $SO_2$ on elemental mercury oxidation over $CeO_2$–$TiO_2$ catalyst. Chem Eng J 219:319–326. doi:10.1016/j.cej.2012.12.100

Liu CX, Chen L, Li JH, Ma L, Arandiyan H, Du Y, Xu JY, Hao JM (2012) Enhancement of activity and sulfur resistance of $CeO_2$ supported on $TiO_2$-$SiO_2$ for the selective catalytic reduction of NO by $NH_3$. Environ Sci Technol 46:6182–6189. doi:10.1021/es3001773

Pirrone N, Cinnirella S, Feng X, Finkelman RB, Friedli HR, Leaner J, Mason R, Mukherjee AB, Stracher GB, Streets DG, Telmer K (2010) Global mercury emissions to the atmosphere from anthropogenic and natural sources. Atmos Chem Phys 10:5951–5964. doi:10.5194/acp-10-5951-2010

Pudasainee D, Lee SJ, Lee SH, Kim JH, Jang HN, Cho SJ, Seo YC (2010) Effect of selective catalytic reactor on oxidation and enhanced removal of mercury in coal-fired power plants. Fuel 89:804–809. doi:10.1016/j.fuel.2009.06.022

Qi G, Yang RT, Chang R (2004) $MnO_x$-$CeO_2$ mixed oxides prepared by co-precipitation for selective catalytic reduction of NO with NH3 at low temperatures. Appl Catal B-Environ 51:93–106. doi:10.1016/j.apcatb.2004.01.023

Qu L, Li C, Zeng G, Zhang M, Fu M, Ma J, Zhan F, Luo D (2014) Support modification for improving the performance of $MnO_x$–$CeO_y$/$\gamma$-Al2$O_3$ in selective catalytic reduction of NO by NH3. Chem Eng J 242:76–85. doi:10.1016/j.cej.2013.12.076

Shang X, Hu G, He C, Zhao J, Zhang F, Xu Y, Zhang Y, Li J, Chen J (2012) Regeneration of full-scale commercial honeycomb monolith catalyst ($V_2O_5$–$WO_3$/$TiO_2$) used in coal-fired power plant. J Ind Eng Chem 18:513–519. doi:10.1016/j.jiec.2011.11.070

Shen B, Wang F, Liu T (2014a) Homogeneous $MnO_x$-$CeO_2$ pellets prepared by a one-step hydrolysis process for low-temperature $NH_3$-SCR. Powder Technol 253:152–157. doi:10.1016/j.powtec.2013.11.015

Shen B, Wang Y, Wang F, Liu T (2014b) The effect of Ce-Zr on $NH_3$-SCR activity over $MnO_{x(0.6)}$/$Ce_{0.5}Zr_{0.5}O_2$ at low temperature. Chem Eng J 236:171–180. doi:10.1016/j.cej.2013.09.085

Singh S, Nahil MA, Sun X, Wu C, Chen J, Shen B, Williams PT (2013) Novel application of cotton stalk as a waste derived catalyst in the low temperature SCR-deNOx process. Fuel 105:585–594. doi:10.1016/j.fuel.2012.09.010

Srivastava RK, Hutson N, Martin B, Princiotta F, Staudt J (2006) Control of mercury emissions from coal-fired in electric utility boilers. Environ Sci Technol 40:1385–1393. doi:10.1021/es062639u

Svachula J, Alemany LJ, Ferlazzo N, Forzatti P, Tronconi E, Bregani F (1993) Oxidation of sulfur dioxide to sulfur trioxide over honeycomb DeNoxing catalysts. Ind Eng Chem Res 32:826–834. doi:10.1021/ie00017a009

Tan Z, Su S, Qiu J, Kong F, Wang Z, Hao F, Xiang J (2012) Preparation and characterization of $Fe_2O_3$–$SiO_2$ composite and its effect on elemental mercury removal. Chem Eng J 195–196:218–225. doi:10.1016/j.cej.2012.04.083

Tao S, Li C, Fan X, Zeng G, Lu P, Zhang X, Wen Q, Zhao W, Luo D, Fan C (2012) Activated coke impregnated with cerium chloride used for elemental mercury removal from simulated flue gas. Chem Eng J 210:547–556. doi:10.1016/j.cej.2012.09.028

Wang P, Su S, Xiang J, You H, Cao F, Sun L, Hu S, Zhang Y (2014) Catalytic oxidation of $Hg^0$ by $MnO_x$–$CeO_2$/$\gamma$-$Al_2O_3$ catalyst at low temperatures. Chemosphere 101:49–54. doi:10.1016/j.chemosphere.2013.11.034

Wiatros-Motyka MM, C-g S, Stevens LA, Snape CE (2013) High capacity co-precipitated manganese oxides sorbents for oxidative mercury capture. Fuel 109:559–562. doi:10.1016/j.fuel.2013.03.019

Wu Z, Jin R, Liu Y, Wang H (2008) Ceria modified $MnO_x$/$TiO_2$ as a superior catalyst for NO reduction with $NH_3$ at low-temperature. Catal Commun 9:2217–2220. doi:10.1016/j.catcom.2008.05.001

Xu H, Zhang Q, Qiu C, Lin T, Gong M, Chen Y (2012) Tungsten modified MnOx–CeO2/ZrO2 monolith catalysts for selective catalytic reduction of NOx with ammonia. Chem Eng Sci 76:120–128. doi:10.1016/j.ces.2012.04.012

Yan NQ, Chen WM, Chen J, Qu Z, Guo YF, Yang SJ, Jia JP (2011) Significance of $RuO_2$ modified SCR catalyst for elemental mercury oxidation in coal-fired flue gas. Environ Sci Technol 45:5725–5730. doi:10.1021/es200223x

Yang S, Guo Y, Yan N, Wu D, He H, Xie J, Qu Z, Jia J (2011a) Remarkable effect of the incorporation of titanium on the catalytic activity and $SO_2$ poisoning resistance of magnetic Mn–Fe spinel for elemental mercury capture. Appl Catal B-Environ 101:698–708. doi:10.1016/j.apcatb.2010.11.012

Yang SJ, Guo YF, Yan NQ, Wu DQ, He HP, Qu Z, Jia JP (2011b) Elemental mercury capture from flue gas by magnetic Mn-Fe spinel: effect of chemical heterogeneity. Ind Eng Chem Res 50:9650–9656. doi:10.1021/ie2009873

Zhang S, Li H, Zhong Q (2012) Promotional effect of F-doped $V_2O_5$-$WO_3$/$TiO_2$ catalyst for $NH_3$-SCR of NO at low-temperature. Appl Catal a-Gen 435:156–162. doi:10.1016/j.apcata.2012.05.049

Zhang X, Shen B, Wang K, Chen J (2013) A contrastive study of the introduction of cobalt as a modifier for active components and supports of catalysts for $NH_3$-SCR. J Ind Eng Chem 19:1272–1279. doi:10.1016/j.jiec.2012.12.028

Zhao B, Liu X, Zhou Z, Shao H, Wang C, Si J, Xu M (2014) Effect of molybdenum on mercury oxidized by $V_2O_5$–$MoO_3$/$TiO_2$ catalysts. Chem Eng J 253:508–517. doi:10.1016/j.cej.2014.05.071

Zhibo X, Chunmei L, Dongxu G, Xinli Z, Kuihua H (2013) Selective catalytic reduction of $NO_x$ with $NH_3$ over iron–cerium mixed oxide catalyst: catalytic performance and characterization. J Chem Technol Biot 88:1258–1265. doi:10.1002/jctb.3966

Zhou J, Hou W, Qi P, Gao X, Luo Z, Cen K (2013) $CeO_2$–$TiO_2$ sorbents for the removal of elemental mercury from syngas. Environ Sci Technol 47:10056–10062. doi:10.1021/es401681y